Subaru Near-Infrared Multicolor Images of Class II Young Stellar Object, RNO 91

Mayama, Satoshi ; Tamura, Motohide ; Hayashi, Masahiko ; Itoh, Yoichi ; Ishii, Miki ; Fukagawa, Misato ; Hayashi, Saeko S. ; Oasa, Yumiko ;…

(Citation)
Publications of the Astronomical Society of Japan,59(6):1153-1160

(Issue Date)
2007-12-25

(Resource Type)
journal article

(Version)
Version of Record

(URL)
https://hdl.handle.net/20.500.14094/90001428

PASJ: Publ. Astron. Soc. Japan **59**, 1153–1160, 2007 December 25

Subaru Near-Infrared Multicolor Images of Class II Young Stellar Object, RNO 91*

Satoshi MAYAMA,[1,2] Motohide TAMURA,[1,3] Masahiko HAYASHI,[1,2] Yoichi ITOH,[4] Miki ISHII,[2] Misato FUKAGAWA,[5] Saeko S. HAYASHI,[1,2] Yumiko OASA,[4] and Tomoyuki KUDO[1,3]

[1]*School of Mathematical and Physical Science, Graduate University for Advanced Studies, 650 North A'ohoku Place, Hilo, HI 96720, USA*

[2]*Subaru Telescope, National Astronomical Observatory of Japan, 650 North A'ohoku Place, Hilo, HI 96720, USA*

[3]*Optical and Infrared Astronomy Division, National Astronomical Observatory of Japan, 2-21-1 Osawa, Mitaka, Tokyo 181-8588*

[4]*Graduate School of Science and Technology, Kobe University, 1-1 Rokkodai-cho, Nada-ku, Kobe 657-8501*

[5]*Division of Particle and Astrophysical Sciences, Nagoya University, Furo-cho, Chikusa-ku, Nagoya 464-8602*

mayamast@subaru.naoj.org

(Received 2007 January 10; accepted 2007 August 23)

Abstract

We conducted subarcsecond near-infrared imaging observations of RNO 91 with CIAO (Coronagraphic Imager with Adaptive Optics) mounted on the 8.2 m Subaru telescope. We present our *JHK* band data along with optical images, which when considered together reveal a complex circumstellar structure. We examined the colors of associated nebulae and compared the geometry of the outflow/disk system suggested by our data with that already proposed on the basis of previous studies. Our *K*-band image shows bright circumstellar nebulosity detected within $\sim 2''$ around the central source, while it is less conspicuous at shorter wavelengths. PA and the size of this red color nebulosity agree with those of the previously detected polarization disk. Agreements among these data indicate that this bright nebulosity region, which follows the reddening law, might be attributed to a disklike structure. At *J* and optical wavelengths, several blue knotlike structures are detected around and beyond the bright circumstellar nebulosity. We suggest that these knotty reflection nebulae may represent disintegrating fragments of an infalling envelope. The three-color composite image has the appearance of arc-shaped nebulosity. We interpret these structures as being roots of a bipolar cavity opening toward the northeast and the southwest. The complex distribution of reflection nebulosity seen around RNO 91 appears to confirm the interpretation that this source is an object dispersing its molecular envelope while transitioning from protostar to T Tauri star.

Key words: ISM: reflection nebula — stars: individual (RNO 91) — stars: pre-main sequence

1. Introduction

RNO 91 is located in the L 43 dark cloud in Ophiuchus at a distance of 160 pc (Herbst & Warner 1981). L 43 is a typical site of low-mass star formation. The cloud houses at least two young nebulous stars (RNO 91 and RNO 90, Cohen 1980). RNO 91 is an embedded source identified as a T Tauri star (Levreault 1988; André & Montmerle 1994). It is classified as an M 0.5 type T Tauri star, which has a mass of 0.5 $M_\odot$ (Levreault 1988). RNO 91 lies within a parabolic-shaped region of lower extinction with a higher surface brightness rim than elsewhere in the L 43 cloud, which Mathieu et al. (1988) referred to as the "bay". The bay opens toward the south, while RNO 91 lies near the closed northern end.

RNO 91 is known as a source of complex molecular outflows (Myers et al. 1988; Mathieu et al. 1988; Parker et al. 1988). The molecular outflow shows spatially separated redshifted and blueshifted lobes. The redshifted-outflow lobe extends to the north, while the blueshifted-outflow lobe extends to the south (Levreault 1988; Myers et al. 1988; Mathieu et al. 1988). Since the outflow velocities are only a few km/s from systemic velocity assuming an outflow inclination angle of 20°–30° to the plane of the sky, it is difficult to reconcile these low velocities with either jet or wind model (Lee et al. 2002). CO $J = 2$–1 observations toward the outflow show weak low-velocity emission along the outflow axis at about $500''$ away from the source (Bence et al. 1998). Lee and Ho (2005) presented maps of the integrated CO $J = 1$–0 emission, which also showed that the southeast lobe appeared as a U-shaped shell extending over $\sim 500''$ southeastward. Inside the southeastern lobe, CO structures consisting of a chain of knotty structures are seen along the axis (Lee & Ho 2005). Recent high-resolution radio observations revealed the inner region within $30''$ of the source, and showed the presence of compact outflows (Arce & Sargent 2006).

Previous near-infrared and optical observations suggested that RNO 91 is associated with a reflection nebula (Schild et al. 1989; Hodapp 1994; Weintraub et al. 1994) and shock-excited H_2 emission (Kumar et al. 1999). Previous radio observations revealed that RNO 91 is associated with an ammonia envelope (Mathieu et al. 1988) and HCO^+ and N_2H^+ envelopes (Lee & Ho 2005).

Optical and infrared photometry (from *U* band to *L* band) was obtained by Myers et al. (1987). Schild, Weir, and Mathieu (1989) presented optical images of this object and noted that

* Based on data collected at the Subaru Telescope, which is operated by the National Astronomical Observatory of Japan.

the extended structure in their images is aligned perpendicular to the outflow and might be attributed to material associated with a disklike structure. This disklike structure seems to extend to 1000–2000 AU. Scarrott, Draper, and Tadhunter (1993) presented an optical polarization map of the small-scale nebula surrounding RNO 91, and also suggested the presence of a small-scale, few arcsec circumstellar disk, which has collimated the outflow leading to the visible nebula. Weintraub et al. (1994) demonstrated with their K-band polarimetric image that RNO 91 is surrounded by an edge-on circumstellar disklike structure of radius 1700 AU. However, the geometry of RNO 91, especially its inner region ($\sim 20''$), is not well confirmed yet. RNO 91, even though in the late stages of star formation, is still active in producing an outflow. Outflows play an important role in the star-formation process through their strong physical impact on the environments of young stellar objects. Thus, the L 43/RNO 91 system is one of the best targets for studying these interactions, such that how an outflow may reduce and disperse an infalling envelope. High-resolution imaging is needed to understand the geometry of RNO 91 in the innermost region and the interaction between the outflow and the disk. Furthermore, RNO 91 is an important candidate because it is considered to be a YSO in a transition phase between a protostar and a visible pre–main-sequence star (Parker 1991).

In this paper, we present subarcsecond near-infrared and optical images of RNO 91 obtained with the Subaru telescope, and discuss the morphology of circumstellar structures associated with RNO 91. Observations and data-reduction procedures are described in sections 2 and 3, respectively. Results and discussion are presented in sections 4 and 5, respectively. Section 6 summarizes the conclusions.

2. Observations

Infrared observations were carried out on 2001 May 15 with the Coronagraphic Imager with Adaptive Optics, CIAO (Tamura et al. 2000; Murakawa et al. 2004), mounted at the f/12 Cassegrain focus of the 8.2 m Subaru telescope. The pixel scale and the orientation of the 1024×1024 InSb array (ALADDIN II) were measured using the Trapezium (Simon et al. 1999) with the same optical configurations for the RNO 91 observations, and were $0\farcs0213 \pm 0\farcs0003$ pixel^{-1} (Itoh et al. 2005) and $5\fdg7 \pm 0\fdg8$, respectively. The field of view was $22'' \times 22''$. Imaging observations were carried out in the J, H, and K bands centered at 1.25, 1.65, and 2.2 μm, respectively. The sky was clear and photometric, and the seeing was stable. Adaptive optics was not used due to an unavailability of appropriate natural guide stars. An occulting mask was not used. The PSFs of the point source observed in the same night have sizes of $0\farcs4 \pm 0\farcs1$ (FWHM).

We obtained 6 frames with 10 s $\times$ 3 coadds, 10 s $\times$ 3 coadds and 5 s $\times$ 6 coadds for the J, H, and K bands, respectively. The photometric standard star FS 141 (Hawarden et al. 2001) data and sky frames were obtained after observations of RNO 91. Dome flats and dark frames were taken at the end of the night.

Additional infrared observations were carried out on 2005 June 27 with CIAO. The average natural seeing was $0\farcs5$. The pixel scale and the position angle of the detector were $0\farcs0213 \pm 0\farcs0001$ pixel^{-1} and $1\fdg68 \pm 0\fdg27$ (Mayama et al. 2006). We obtained 40, 80, and 3 frames for RNO 91 with 10 s $\times$ 1 coadds, 1 s $\times$ 1 coadds, and 0.33 s $\times$ 40 coadds for the J, H, and K bands, respectively. No photometric standard star was observed. Dome flats and dark frames were taken at the end of the night.

Hubble Space Telescope (HST) archive data that was already calibrated was also used. The observations were carried out on 1999 January 21 with the WFPC2 (Wide Field Planetary Camera 2). WFPC2 consists of Wide Field camera (WF3) and Planetary Camera (PC1). RNO 91 was imaged with a F606W filter. The pixel scales of WF3 and PC1 are $0\farcs1$ pixel^{-1} and $0\farcs046$ pixel^{-1}, respectively. The fields of view of WF3 and PC1 are $2\farcm5 \times 2\farcm5$ (L-shaped) and $35'' \times 35''$, respectively. The total integration times of WF3 and PC1 are 300 s and 100 s, respectively.[1]

3. Data Reduction

The Image Reduction and Analysis Facility (IRAF) software was used for all data reduction. A dark frame was subtracted from each object frame, which was then divided by the dome-flat. Hot and bad pixels were removed and the sky frame was subtracted. We combined the frames of each band to produce the final images.

The J-, H-, and K-band images of RNO 91 are presented in figure 1 together with an HST-WFPC2 (WF3) optical image. The J-band image is from our second observations (in 2005), while the H-and K-band images are from our first observations (in 2001). The instrumental magnitude was used to calculate the value [mJy/arcsec^2] for the J-band image in figure 1, as no photometric standard star was observed during our observations in 2005. Identifiers of each structural feature are noted in figure 4.

Changing the band filters of CIAO during an observation introduces a slight displacement of the object's position on the detector. Measuring precise positions of the central source is essential in comparing the structures among different wavelength images, such as making color composite images and identifying structures. However, it is hard to precisely measure the positions of the central source, which is deeply embedded in circumstellar material, or spatially elongated, such as RNO 91. Furthermore, in the RNO 91 images, there are no background point sources to which we can refer. Although there is a peak-intensity position that we are able to measure, their positions could differ in each different band.

In order to overcome this problem, we adopted the following method to correct for any displacement in position on the detector at different wavelength images. First, the peak position of the point source that was observed at J, H, and K on the same night with RNO 91 were measured. Second, we examined the displacement in the positions of the peaks at different wavelengths. Between the K band and the H band, the derived displacements in position on a detector were

[1] Based on observations made with the NASA/ESA Hubble Space Telescope, obtained at the Space Telescope Science Institute, which is operated by the Association of Universities for Research in Astronomy, Inc., under NASA contract NAS 5-26555.

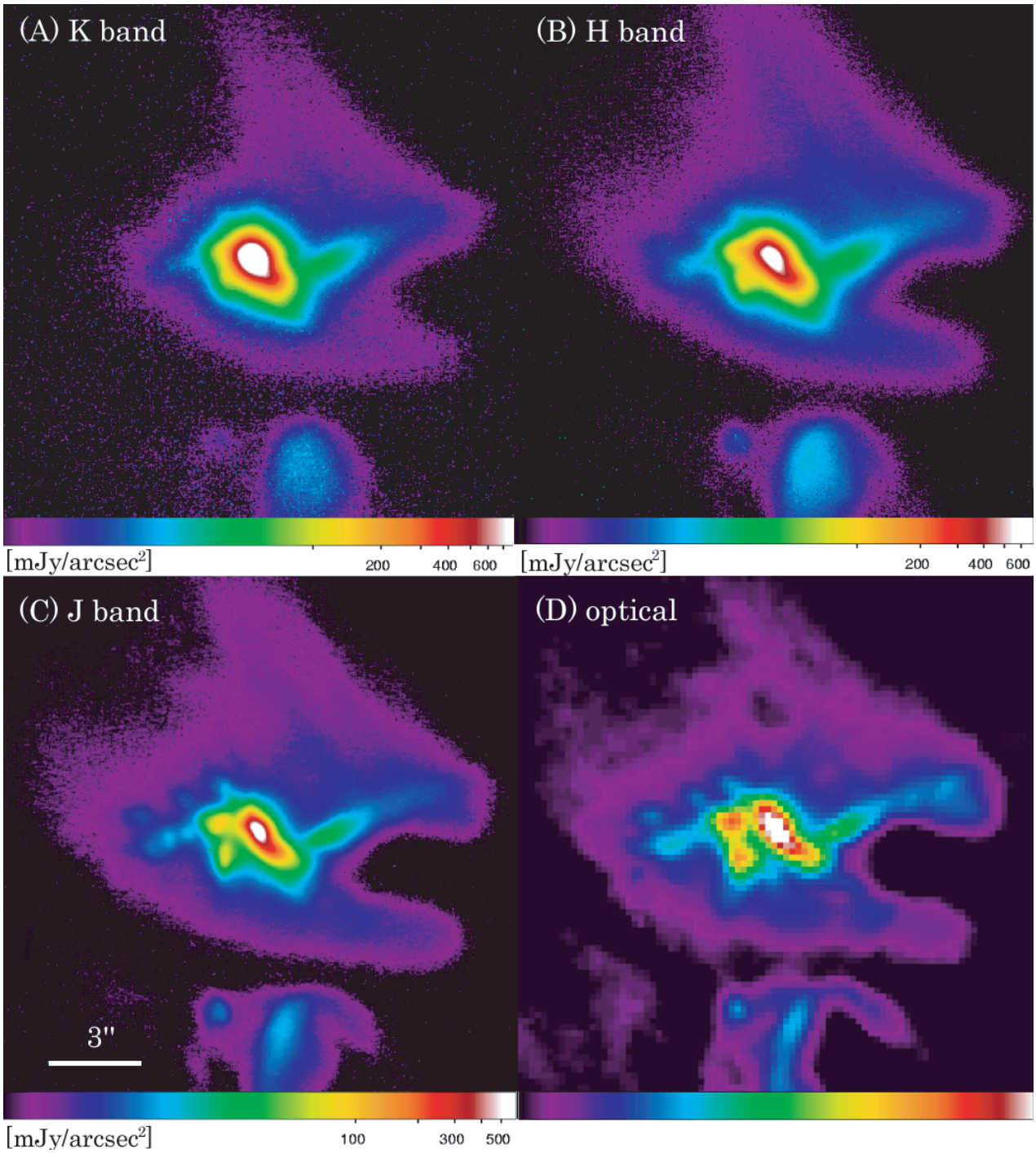

Fig. 1. J-, H-, and K-band images of RNO 91 with an HST optical image (F606W). The field of view (FOV) is $17'' \times 17''$. North is up and east to left.

0.45 ± 0.76 [pixels] at the E–W direction and 0.48 ± 0.14 [pixels] at the N–S direction. Between the H band and the J band, the derived displacements in position on a detector were 0.11 ± 0.78 [pixels] at the E–W direction and 2.4 ± 0.76 [pixels] at the N–S direction. Third, we used these values to shift the images of RNO 91 in order to correct the position displacement on a detector. Finally, the shifted images were used to make color composite images (figure 2).

We lastly address the method of position registration between Subaru and HST images. In order to make three-color composite images, the structural feature identified as V in figure 4 was used for position registration due to the following reasons: (i) There is no background star that can be used for position registration between Subaru and HST images. (ii) The peak positions of V are located at the same position on J-, H-, and K-band images, whose position displacements were already corrected by the method explained in the above paragraph. (iii) The Subaru J-band image is very similar to the HST optical image. These facts enable us to assume that the position of V does not differ among wavelengths. A position

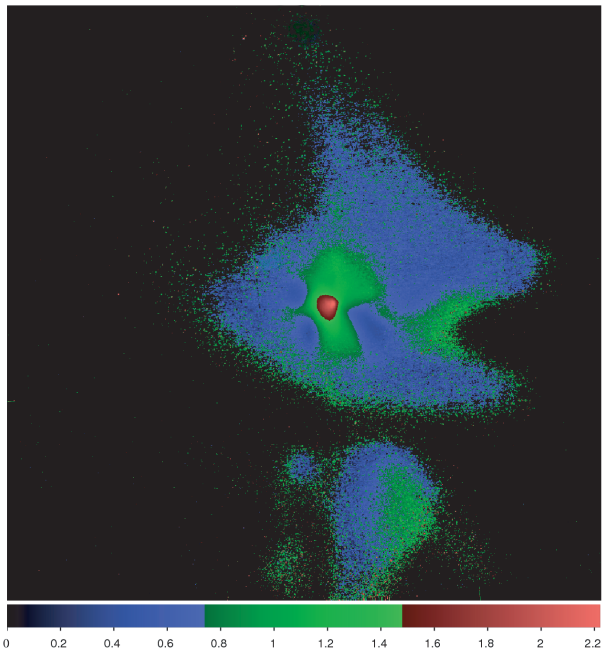

Fig. 2. $H-K$ color image. FOV is $22''\times22''$. North is up and east to left. Strong emission indicates red color and weak emission indicates blue color. The unit of the color bar is magnitude.

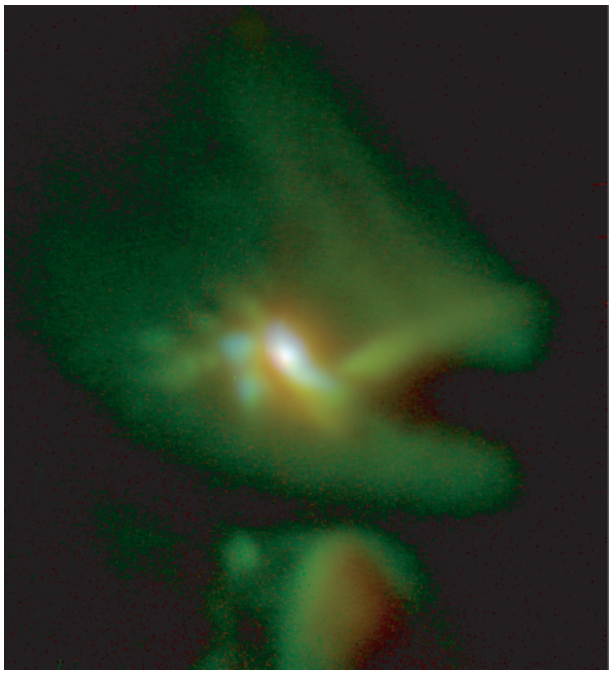

Fig. 3. Three-color composite image of RNO 91. The CIAO K band is registered as red, CIAO J band as green, and WFPC2 optical as blue. North is up and east to left. Note that HST image, whose resolution was degraded to the Subaru level, was used to make this three-color composite image.

uncertainty between the bands is stated in subsection 4.1.

4. Results

4.1. Colors of RNO 91

Figure 2 shows a $H-K$ color image of RNO 91. In this figure, strong emission indicates the red region, while weak emission indicates the blue region. Notable color features in this figure are as follows. The color within a distance of $\sim2''$ from the photocenter of the nebula appears to be red ($H-K>1.1$), while the color beyond a distance of $\sim2''$ from the photocenter of the nebula appears to be blue ($H-K<0.7$). An interpretation of these colors is given in subsection 5.1. Figure 3 shows a three-color composite image of Subaru-CIAO(K), Subaru-CIAO(J), and HST-WFPC2(F606W) broadband observations of RNO 91. Note that figure 3 is composed of images from multiple epochs separated in time by years. The CIAO K band is registered as red, the CIAO J band as green, and WFPC2 F606W as blue. Also note that our $H-K$ color image (figure 2) and the three-color composite image (figure 3) have position uncertainties of up to $0\farcs02$ and $0\farcs1$ due to the issue discussed in the previous section, respectively. However, these uncertainties are small enough to discuss the morphology of the circumstellar structure surrounding RNO 91. In section 5, we explain the details and interpret the features of figures 2 and 3.

4.2. Radial Surface Brightness Profile

Figure 5 shows radial profiles of the surface brightness of RNO 91 associated nebula with respect to the K-band peak position. Data obtained in 2001 were used for all J-, H-, and K-band profiles in figure 5, since no photometric standard star was observed during our 2005 observations. RNO 91 is comprised of several clumps, or knotlike structures. In order to eliminate the effect of such local clump structures, we

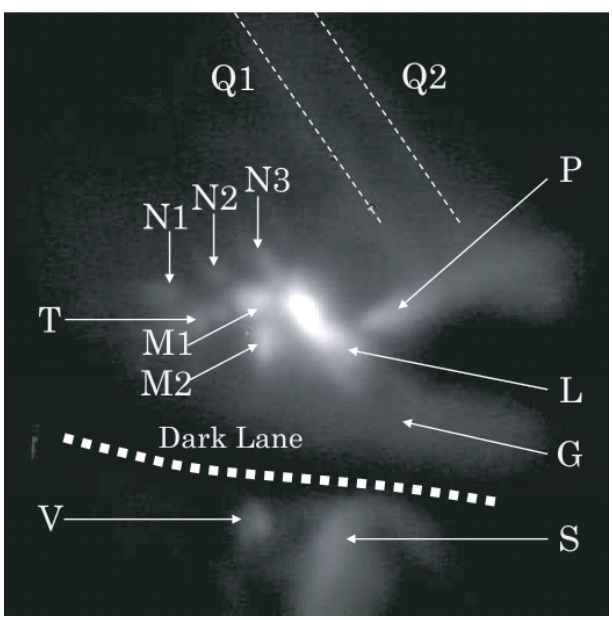

Fig. 4. Identifiers of each structure superimposed on the Subaru J band image. The field of view is $17''\times17''$. M1, M2, N1, N2, and N3 are knotlike structures around the source. Q1 and Q2 are northern arcs. T is eastern arc. P and G are west and southwest arcs, respectively. S is an arc ridge surrounding a southern clump. P, G, and S were initially labeled by Schild, Weir, & Mathieu (1989).

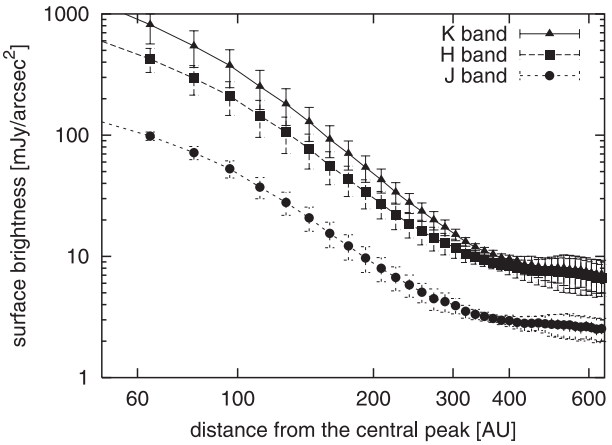

Fig. 5. Radial profile of the surface brightness of RNO 91 associated nebula in the *JHK* band. The statistical error and standard deviation among various orientations were calculated to estimate error bars.

examined the radial surface brightness only along lines of PA = 0°, 30°, 300°, and 330°. The surface brightness decreases as $r^{-2.1\pm0.2}$, $r^{-2.3\pm0.2}$, and $r^{-2.5\pm0.2}$ with the radius r of 48 to 300 AU, for the J, H, and K bands, respectively. The surface brightness decreases as $r^{-0.5\pm0.2}$, $r^{-0.6\pm0.2}$, and $r^{-0.8\pm0.2}$ with the radius r of 300 to 688 AU, for the J, H, and K bands, respectively. The power-law dependence revealed the following points: (1) At all wavelengths, the profile showed a change of slope at $\sim 2''$ (300AU) from the central peak, suggesting a morphological difference beyond this point. (2) The power-law dependence at J, H, and K did not show a significant difference among wavelengths, indicating that the same scatter and absorption were occurring at all wavelengths, regardless of the sizes of dust.

5. Discussion

The complex circumstellar structure was detected in the most inner region ($\sim 20''$), as shown in figures 1 and 3. Figure 6 is a schematic description of the morphology of RNO 91.

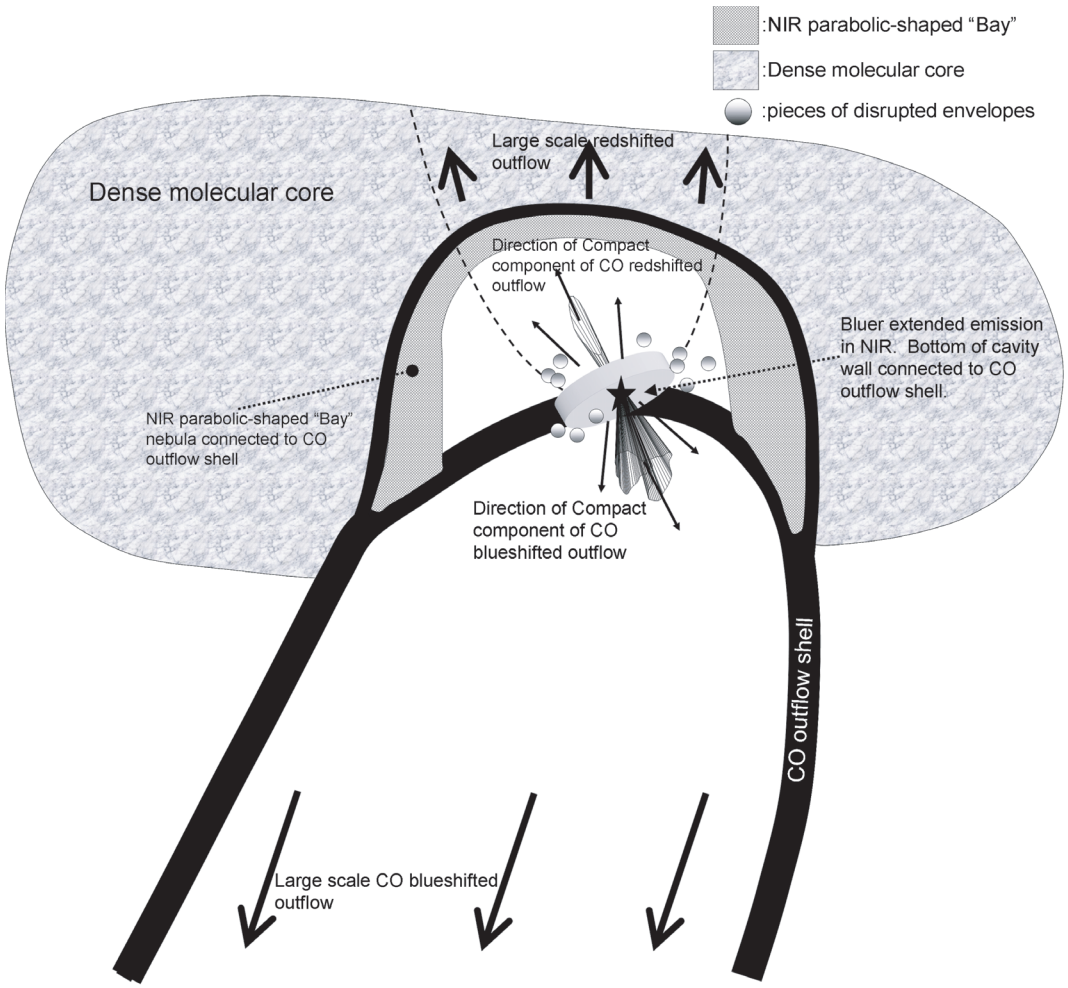

Fig. 6. Illustration of the front view of RNO 91 and its surrounding. The position of the central source is marked by the star. The hatched regions represent compact components of molecular outflow resolved by Arce and Sargent (2006). The shaded area represents near-infrared parabolic shaped "bay" reflection nebulosity seen at optical and near-infrared wavelengths. The sizes of disk, outflow, and molecular core are not drawn with the same scale. The field of view of our Subaru images covers immediate circumstellar environment around the central source such as disk and roots of a bipolar cavity.

5.1. Circumstellar Disklike Structure and Envelope

The K-band image shows bright circumstellar nebulosity detected within $\sim 2''$ around the central source, while less nebulosity is seen at shorter wavelengths, such as J and optical (see figure 1). The nebula appears to become more isotropic with increasing wavelength. Figure 2 shows much red color particularly in the northern part of this bright circumstellar nebulosity, detected within $\sim 2''$ around the central source. The examined $H-K$ and $J-K$ colors around this northern part of bright circumstellar nebulosity are about 1.1–1.2 and 2.9–3.2, respectively. Our $H-K$ and $J-K$ colors for this part can be well explained by the reddening law, while assuming an intrinsic color of an M 0.5 star.

Here, we would like to interpret that this bright circumstellar nebulosity region might be attributed to a disk-like structure, based on following reasons: (1) Scarrott, Draper, and Tadhunter (1993) presented polarization maps of the RNO 91 nebulosity and showed evidence for a small-scale (a few arcsec) circumstellar disk running in a southeast–northwest dircetion. Our $H-K$ color map shows a reddish region ($H-K > 1.1$, figure 2) that extends northwestward along the PA of the putative polarization disk. Therefore, the direction of this red-color region in our $H-K$ image is consistent with PA of their polarization disk. (2) The radial surface brightness profile (figure 5) shows a change of slope at $\sim 2''$ from the photocenter of the nebula, as mentioned in the previous section, quantitatively demonstrating a morphological difference beyond this point. In terms of color, an inner region ($< 2''$) has much redder color than an outer region ($> 2''$). The change in slope of the radial surface profile at a distance of $\sim 2''$ from the photocenter of the nebula appears to agree with the size scale (a few arcsec) of the previously detected polarization disk (Scarrott et al. 1993). Agreements among these data indicate that this bright circumstellar nebulosity region, which follows the reddening law, might be attributed to a disklike structure. In order to confirm this matter, however, further observations in radio wavelength are needed to obtain velocity distribution data of this innermost circumstellar structure.

At J and optical wavelengths, several blue knotlike newly found structures (M1, M2, N1, N2, and N3 in figure 4) are detected around and beyond the bright circumstellar nebulosity. Schild, Weir, and Mathieu (1989) conducted spectroscopic observations toward RNO 91, and did not detect any emission lines in their spectra of the nebular features, except for the bright Hα also seen in RNO 91. They concluded that the nebular feature is mostly, and likely entirely, reflection light from RNO 91, and not from other emission sources. The positions of these blue knots are measured in our images and compared with those in images obtained by Schild, Weir, and Mathieu (1989). These positions are almost consistent, and our images showed spatially well-resolved knots. Thus, as suggested by Schild, Weir, and Mathieu (1989), these blue knots seen in our shorter wavelength images are not other emission sources, but part of reflection nebula.

The tendency of scattered light to be blue (Sellgren et al. 1992) can well explain our colors ($H-K < 0.7$, figure 2) for the knots and reflection nebula. Furthermore, these blue knots seen in our images spread over a region comparable in size to the envelope detected in HCO^+ $J = 1$–0 emission ($\sim 10''$) surrounding RNO 91 (Lee & Ho 2005). It is thus natural to interpret that these knotty reflection nebulae located beyond $2''$ from the central-source position may represent disintegrating fragments of an infalling envelope, as postulated by Mathieu et al. (1988) and Lee and Ho (2005). We are looking at a site where the outflow disrupts an envelope in transition-phase YSOs. Mathieu et al. (1988) suggested that the molecular outflow is disrupting the dense core in L 43, and it may well be that the clumps are part of this erosion. Lee and Ho (2005) also detected clumps or knotlike structures around the central peak, and interpreted them as being fragments, or part of erosion that occurred in envelope structures, which are disrupted by molecular outflow. These previous studies support our interpretation.

5.2. Outflow and Cavity

Figure 3 has the appearance of arc-shaped nebulosity extending northward and eastward through the central source (Q1, Q2, and T in figure 4). The northern ridge is $11''$ long and the eastern one is $7''$ long. On the other end of this arc-shaped structure, the nebula appears to become more extended ($2\farcs3$ long) southwestward (PA $\sim 225°$) from the central-source position in the J band and HST optical images (see figure 1 and L in figure 4), then branching to two lobes (P and G in figure 4) with an apparent cavity. Regarding the inner part within $2''$ to $3''$ from the central-source position, our $H-K$ color (figure 2) and three-color composite image (figure 3) shows that only this southwestern direction has the blue ($H-K < 0.6$) extended feature, while the other directions have much redder ($H-K > 1.1$) circular structure, which we interpreted as a disklike structure in the previous section. This color distribution indicates that the extinction in the southwestern direction from the central-source position is less than the counterpart. This extinction structure requires a geometry such that the southwestern direction is the near side. This also requires that the southwestern outflow needs to be the near side. Therefore, we interpret these whole structures as being roots of a bipolar cavity opening toward the southwest (near side) and the northeast (far side).

There are four arguments presented in previous papers that support our suggestion about geometry. First, Scarrott, Draper, and Tadhunter (1993) detected a polarization disk that collimated the outflow leading to the visible nebula. Their orientation of the polarization disk was 145°, and an outflow axis that is collimated by this disk needs to be perpendicular to this orientation. Hence, an orientation of extended nebula in our J band and HST optical images (marked as L & G in figure 4) is almost consistent with that of blueshifted-outflow axis derived by Scarrott, Draper, and Tadhunter (1993).

Second, Lee and Ho (2005) mapped N_2H^+ $J = 1$–0 emission, and showed that there is more N_2H^+ emission extending northeastward, while less N_2H^+ emission extending southwestward (figure 1c in Lee & Ho 2005). They suggested that the scarcity of the N_2H^+ emission to the southwest was likely due to less material there. As N_2H^+ mainly traces the dense and cool material in the envelope, this N_2H^+ distribution indirectly suggests a tendency of blueshifted molecular outflow sweeping away material located around the southwest of the

central source.

Third, Kumar, Anandarao, and Davis (1999) reported detection of the H_2 $v = 1$–0 S(1) line at 2.122 μm, and found shock-excited H_2 emission originating in an outflow. In their image, H_2 emission is clearly extended more southward than northward (Kumar et al. 1999). Therefore, the direction of outflow seen in H_2 emission is consistent with the nebulosity seen at our short wavelengths (labeled L in figure 4), indicating that the blueshifted outflow has components extending southward or southwestward.

Fourth, several previous studies presented the CO emission maps that probe the low-density, high-velocity outflow gas originating from RNO 91. Here, we focus on several recent data that show relatively small-scale outflow structures comparable in size to our NIR images. Arce and Sargent (2006) presented ^{12}CO (1–0) mapping in the innermost region with high spatial resolutions (4″ to 6″), which is sensitive to the bright, compact-scale outflow structures within 30″ from the source. In their ^{12}CO ($J = 1$–0) contour maps, blueshifted emission extends southward and southwestward, while redshifted emission extends northward and northeastward. We describe this compact-scale outflow separately in figure 6, because it is slightly shifted with respect to the large-scale outflow that we explain below. Lee and Ho (2005) also mapped the CO $J = 1$–0 emission with a resolution of $\sim$10″. In their small-scale CO map (figure 1b in Lee & Ho 2005), there is blueshifted CO emission extending south-southwestward that traces the outflow axis in their interpretation. Another blueshifted CO emission extending west-southwestward is interpreted as an outflow shell. Figure 5 in Lee et al. (2000) also shows strong emission extending southward and southwestward. These previous studies revealed that there is a CO outflow component extending southwestward in close vicinity to RNO 91. All of these have the same orientation of the blue extended feature seen in our Subaru and HST images. Note that the orientation of the redshifted CO emission seen in Arce and Sargent (2006) also well matches that of our northeastern cavity geometry.

In conjunction with these four features from previous studies, we again suggest that the blue color extended nebulosity seen in our near-infrared images (L, P, and G in figure 4) might be tracing a root of blueshifted outflow cavity, eventually connecting to the CO outflow shell with increasing distance. The arc-shaped nebulosity (Q1, Q2, and T in figure 4) extending northward and eastward through the central source is a counterpart of this cavity. The redshifted molecular outflow might have constructed the northeastern cavity, while the blueshifted molecular outflow might have constructed the southwestern counterpart.

We then turn our focus on the large-scale ($\sim$500″) outflow geometry. Lee et al. (2000) presented the CO $J = 1$–0 emission associated with RNO 91, and found that the molecular outflow has a large-scale southeastern lobe. Their outflow has a wide-opening angle ($\sim$160°) and the centroid of the outflow emission seems to curve eastward with increasing distance from the source. They suggested that there was interaction with ambient material that guides the orientation of the outflow. Alternatively, it could be that the intrinsic outflow axis is changing with time as a result of precession in the exciting source (Lee et al. 2000). Precession of the outflow axis is suggested to occur in a few objects, such as L 1157 and L 723 (Gueth et al. 1996; Hirano et al. 1998; Zhang et al. 2000; Bachiller et al. 2001). From this point of view, there could be an explanation that a bottom of the blueshifted outflow has a component that has a direction toward the southwest in the vicinity of the source, which was seen in our near-infrared images, and then blueshifted outflow curves eastward with increasing distance from the source. This possible interpretation is illustrated in figure 6 as well. However, it is still hard to discern a real sense of the outflow orientation using our data alone, which has a field of view of 20″.

5.3. *South Clump and Dark Lane*

The southern clump (S in figure 4), located 6″–7″ south of the central source, gives the appearance of a blue ($H - K < 0.5$, figure 2) arclike ridge surrounding a red ($H - K > 0.8$, figure 2) inner component. The location of this southern clump in our K-band image coincides well with that of the integrated intensity of ^{13}CO (1–0) emission mapped by Arce and Sargent (2006). Since ^{13}CO (1–0) emission usually traces dense gas, this southern clump in our image can be interpreted as being the circumstellar gas envelope. In some cases of Class II sources, a gaseous component that has been entrained by the outflow may form relatively dense shells and clumps at the edge of the outflow lobe around the source (Arce & Sargent 2006). Therefore, this southern clump could be residues after outflow clears away the surrounding gas.

This south clump is separated from the central source by a gap of 2″. Our $H - K$ color image suggests that this dark lane has no additional reddening here, and thus that this gap might not shadow a disk around RNO 91. Unfortunately, there have been no radio data so far having sufficient resolution to resolve this dark lane. We consider that there is an actual break in the mass distribution here.

6. Summary

We have obtained subarcsecond near-infrared (*JHK* band) images of a Class II source, RNO 91, utilizing the near-infrared camera, CIAO, mounted on the 8.2 m Subaru telescope. We presented *JHK* band and optical images, which are the highest resolution images of RNO 91 ever taken. New insights into the immediate circumstellar environment around RNO 91 are obtained. The main conclusions are as follows:

1. The K-band image shows bright circumstellar nebulosity detected within $\sim$2″ (300AU) around the central source, while it is less conspicuous at shorter wavelengths, such as J and optical. The nebula appears to become more isotropic with increasing wavelength. PA and the size of this much redder color nebulosity in our $H - K$ color image agree with those of the polarization disk previously suggested by Scarrott, Draper, and Tadhunter (1993). Agreements among these data indicate that this bright circumstellar nebulosity region, which follows the reddening law, might be attributed to a disklike structure.

2. At J and optical wavelengths, several blue knotlike structures are detected around and beyond the bright circumstellar nebulosity. These blue knots seen in our images spread over a region comparable in size to the envelope detected in HCO^+ $J = 1$–0 emission ($\sim 10''$) surrounding RNO 91 (Lee & Ho 2005). It is natural to interpret that these knotty reflection nebulae located beyond $2''$ from the central-source position may represent disintegrating fragments of an infalling envelope.

3. Three-color composite image has an appearance of arc-shaped nebulosity extending northward and eastward through the central source. On the other end of this arc-shaped structure, the nebula appears to become more extended ($2''.3$ long) southwestward (PA $\sim 225°$) from the central-source position in the J band and HST optical images. We interpret the whole structures as being roots of a bipolar cavity opening toward the northeast and southwest. Redshifted molecular outflow might have constructed the northeastern cavity, while blueshifted molecular outflow might have created the southwestern counterpart.

4. The southern clump, located $6''\sim 7''$ south of the central source, gives the appearance of a blue arclike ridge surrounding a red inner component. The location of this southern clump in our K-band image coincides well with that of the integrated intensity of ^{13}CO (1–0) emission mapped by Arce and Sargent (2006). This southern clump in our image can be interpreted as being the circumstellar gas envelope. This southern clump is separated from the central source by a gap of $2''$. No $H-K$ color change near the dark lane suggests that this gap might not shadow a disk around RNO 91, but show an actual break in the mass distribution.

We thank the telescope staff members and operators at the Subaru telescope, especially Sumiko Harasawa and Dennis Scarla, for their assistance. We are grateful for having fruitful discussions with Michihiro Takami, Ray Furuya, Takayuki Nishikawa, Takuya Fujiyoshi, Takuya Yamashita, Yasushi Nakajima, and Chin-Fei Lee. We also thank our referee for constructive comments that helped to improve this manuscript. The HST data presented in this paper was obtained from the Multimission Archive at the Space Telescope Science Institute (MAST). These observations are associated with programs 7387 and 8216 conducted by Dr. K. R. Stapelfeldt (Principal Investigator). S. M. is financially supported by Japan Society for the Promotion of Science (JSPS) for Young Scientists.

References

André, P., & Montmerle, T. 1994, ApJ, 420, 837
Arce, H. G., & Sargent, A. I. 2006, ApJ, 646, 1070
Bachiller, R., Pérez Gutiérrez, M., Kumar, M. S. N., & Tafalla, M. 2001, A&A, 372, 899
Bence, S. J., Padman, R., Isaak, K. G., Wiedner, M. C., & Wright, G. S. 1998, MNRAS, 299, 965
Cohen, M. 1980, AJ, 85, 29
Gueth, F., Guilloteau, S., & Bachiller, R. 1996, A&A, 307, 891
Hawarden, T. G., Leggett, S. K., Letawsky, M. B., Ballantyne, D. R., & Casali, M. M. 2001, MNRAS, 325, 563
Herbst, W., & Warner, J. W. 1981, AJ, 86, 885
Hirano, N., Hayashi, S. S., Umemoto, T., & Ukita, N. 1998, ApJ, 504, 334
Hodapp, K.-W. 1994, ApJS, 94, 615
Itoh, Y., et al. 2005, ApJ, 620, 984
Kumar, M. S. N., Anandarao, B. G., & Davis, C. J. 1999, A&A, 344, L9
Lee, C.-F., & Ho, P. T. P. 2005, ApJ, 624, 841
Lee, C.-F., Mundy, L. G., Reipurth, B., Ostriker, E. C., & Stone, J. M. 2000, ApJ, 542, 925
Lee, C.-F., Mundy, L. G., Stone, J. M., & Ostriker, E. C. 2002, ApJ, 576, 294
Levreault, R. M. 1988, ApJ, 330, 897
Mathieu, R. D., Benson, P. J., Fuller, G. A., Myers, P. C., & Schild, R. E. 1988, ApJ, 330, 385
Mayama, S., et al. 2006, PASJ, 58, 375
Murakawa, K., et al. 2004, PASJ, 56, 509
Myers, P. C., Fuller, G. A., Mathieu, R. D., Beichman, C. A., Benson, P. J., Schild, R. E., & Emerson, J. P. 1987, ApJ, 319, 340
Myers, P. C., Heyer, M., Snell, R. L., & Goldsmith, P. F. 1988, ApJ, 324, 907
Parker, N. D. 1991, MNRAS, 251, 63
Parker, N. D., Padman, R., Scott, P. F., & Hills, R. E. 1988, MNRAS, 234, 67P
Scarrott, S. M., Draper, P. W., & Tadhunter, C. N. 1993, MNRAS, 262, 306
Schild, R., Weir, N., & Mathieu, R. D. 1989, AJ, 97, 1110
Sellgren, K., Werner, M. W., & Dinerstein, H. L. 1992, ApJ, 400, 238
Simon, M., Close, L. M., & Beck, T. L. 1999, AJ, 117, 1375
Tamura, M., et al. 2000, Proc. SPIE, 4008, 1153
Weintraub, D. A., Tegler, S. C., Kastner, J. H., & Rettig, T. 1994, ApJ, 423, 674
Zhang, Q., Ho, P. T. P., & Wright, M. C. H. 2000, AJ, 119, 1345